Progress In Electromagnetics Research, Vol. 141, 233–248, 2013

NEW DIELECTRIC 1-D EBG STRUCTURE FOR THE DESIGN OF WIDEBAND RESONATOR ANTENNAS

Naizhi Wang[1, *], Chong Zhang[1], Qingsheng Zeng[2], Naiqiang Wang[3], and Jiadong Xu[1]

[1]School of Electronics and Information, Northwestern Polytechnical University, Xi'an 710072, China

[2]Communication Research Center Canada, Ottawa, Ontario K2H 8S2, Canada

[3]Beijing Aerospace Control Center, Beijing 100094, China

Abstract—In this paper, we propose a method to use 1-D dielectric slabs, instead of metallic Frequency Selective Surfaces (FSSs), to produce Partially Reflective Surfaces (PRSs) with positive reflection phase gradients. The structure is realized by a single kind of dielectric substrate. It is modeled as cascaded transmission lines and then analyzed by virtue of the Smith Chart from the perspective of impedance transformation. A PRS designed by this approach is then applied to the realization of a wideband EBG resonator antenna operating at Ku band which is fed by a slot-coupled patch antenna. The calculated results indicate that the antenna possesses a relative 3 dB gain bandwidth of 22%, from 14.1 GHz to 17.6 GHz, with a peak gain of 17 dBi. The impedance bandwidth for the reflection coefficient (S_{11}) less than -10 dB, is from 14 GHz to 17.7 GHz, well covering the 3 dB gain bandwidth. A prototype has been fabricated and measured, and the experimental results well validate the simulation. The design method developed here is significantly effective, and can be easily adopted for antenna designs at other frequencies.

1. INTRODUCTION

In recent years, the electromagnetic band gap (EBG) structure has attracted considerable interest from the electromagnetic community, with regard to their applications in controlling electromagnetic waves

Received 12 June 2013, Accepted 9 July 2013, Scheduled 13 July 2013

* Corresponding author: Naizhi Wang (naizhiwang@hotmail.com).

as semiconductors control the propagation of electrons [1]. Among them, one particular application is using EBG structures to realize high gain EBG resonator antennas [2–4]. A conventional EBG resonator antenna is formed by suspending an EBG structure as a partially reflective surface (PRS) at a proper distance from a ground plane [5]. The air-filled cavity created between the PRS and the ground plane is then fed by a small antenna or an array. No reflective sidewall is needed when applying such geometry since no propagating transversal mode exists inside the cavity at the operating frequency. The main advantage of this kind of antenna is that it can achieve a high radiation gain without the complex beam-forming network that is essential in an antenna array system and leads to serious metal and dielectric losses, particularly in the millimeter-wave band [6]. However, an inherently narrow gain bandwidth due to narrowband characteristics of both the resonant cavity and the EBG structure severely inhibits its use for many applications. For example, for a directivity of 20 dBi, the bandwidth of mono-source EBG resonator antennas is less than 6%, too narrow for them to be used for most of the telecommunication applications [7, 8]. It has been shown that there is a relationship between the maximum gain and the gain bandwidth which depends on the properties of the EBG materials [8]. Maximum gain can be traded for gain bandwidth by modifying the reflection magnitude of the PRS. It also has been shown that using an antenna array, instead of a single antenna, as the excitation of an EBG resonator antenna can improve the gain bandwidth [9, 10]. By means of this, a gain bandwidth of 13.2% has been reported in [10] while maintaining a high gain over 20 dBi. However, this approach makes the advantages of simplicity and high efficiency of EBG resonator antennas over conventional array antennas disappear. Another method to enhance the gain bandwidth is based on the ray theory analysis [11]. It is found that a wideband EBG resonator antenna could be obtained by using a PRS with a positive reflection phase gradient. This kind of PRS has been realized by a combination of two layers of metallic Frequency Selective Surfaces (FSSs) [12–14]. Designed using this method, an EBG resonator antenna with a 3 dB gain bandwidth of 15.7% and a peak gain of 16.2 dBi has been reported [14]. This approach is preferable because it can enhance the gain bandwidth while keeping the advantages of the EBG resonator antenna.

In this paper, we present a new method to use 1-D dielectric slabs, instead of metallic FSSs, to produce PRSs with positive reflection phase gradients. The structure is realized by a single kind of dielectric substrate. It is modeled as cascaded transmission lines and then analyzed by virtue of the Smith Chart from the perspective of

impedance transformation. A PRS designed by this approach is then applied to the design of a wideband EBG resonator antenna operating at Ku band. The antenna is fed by a slot-coupled patch antenna with a wide impedance bandwidth ($S_{11} < -10\,\text{dB}$). The patch antenna is air-loaded between the patch and the slot to suppress the excitation of surface waves, which can be introduced to the cavity and degrade the performance of the EBG resonator antenna. To validate the method and analysis, a prototype is fabricated and measured, and simulated and measured results are compared and discussed.

The organization of this paper is as follows. In Section 2 the brief ray theory analysis of the EBG resonator antenna is presented. In Section 3, the design approach of the 1-D EBG structure with a positive reflection phase gradient is demonstrated. Section 4 describes the design of the feeding patch antenna as well as the overall design of the EBG resonator antenna; comparisons between simulation and measurement are also carried out in this section. Finally, Section 5 concludes the paper.

2. RAY THEORY ANALYSIS

The antenna was initially analyzed with a ray theory approach [15], and it is very helpful for understanding the operating principle. Here we provide the concise derivation procedure in order to obtain the reflection phase relationship which should be satisfied to form a wideband EBG resonator antenna. The schematic diagram of the antenna is shown in Fig. 1. The radiation of the feeding source located in front of the metal ground plane can be imagined as originating in a center point with element pattern $F(\theta)$ and maximum electric field magnitude E_0. A PRS placed at a distance of h from the ground plane introduces multi-reflections with tapered magnitude between the two

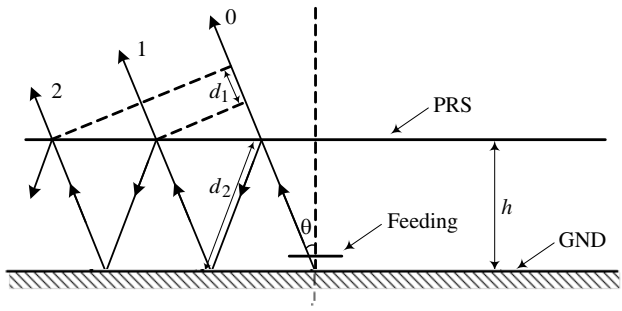

Figure 1. Ray-tracing model of the antenna.

planes. The reflection coefficient of the PRS is $\rho e^{j\varphi}$, where ρ is the magnitude and φ is the reflection phase. Assuming the dimension of the antenna to be infinite and no transmission losses, the magnitude of the ray 0 is proportional to $\sqrt{1-\rho^2}$; the magnitude of the once-reflected ray 1 is proportional to $\rho\sqrt{1-\rho^2}$; the magnitude of the twice-reflected ray 2 is proportional to $\rho^2\sqrt{1-\rho^2}$; etc.. According to the geometric relationship, we obtain

$$d_1 = 2h\tan\theta\sin\theta = 2h\left(\frac{1}{\cos\theta} - \cos\theta\right) \tag{1}$$

$$d_2 = \frac{h}{\cos\theta} \tag{2}$$

Considering the phase variations during reflections from the metal ground plane and the PRS, and also the path differences of rays, the total phase difference between ray 1 and ray 0 can be written as

$$\Delta_1 = \frac{2\pi}{\lambda}d_1 - \frac{2\pi}{\lambda}2d_2 - \pi + \varphi = \varphi - \pi - \frac{4\pi}{\lambda}h\cos\theta \tag{3}$$

The phase difference between ray 2 and ray 0 can be written as

$$\Delta_2 = \frac{2\pi}{\lambda}2d_1 - \frac{2\pi}{\lambda}4d_2 - 2\pi + 2\varphi = 2\left[\varphi - \pi - \frac{4\pi}{\lambda}h\cos\theta\right] \tag{4}$$

And further we derive the general phase difference relationship

$$\Delta_n = n\phi = n\left[\varphi - \pi - \frac{4\pi}{\lambda}h\cos\theta\right] \tag{5}$$

In the far field, the electric field intensity is written as the vector sum of all the rays

$$E = \sum_{n=0}^{\infty} F(\theta)E_0\rho^n\sqrt{1-\rho^2}e^{j\Delta_n} \tag{6}$$

Since $\rho < 1$, we obtain

$$\sum_{n=0}^{\infty}\rho^n e^{j\Delta_n} = \sum_{n=0}^{\infty}\left(\rho e^{j\phi}\right)^n = \frac{1}{1-\rho e^{j\phi}} \tag{7}$$

Then the absolute value of far field strength is

$$|E| = |E_0|\,F(\theta)\sqrt{\frac{1-\rho^2}{1+\rho^2-2\rho\cos\phi}} \tag{8}$$

and the power pattern is

$$S = \frac{1-\rho^2}{1+\rho^2-2\rho\cos\left(\varphi-\pi-\frac{4\pi}{\lambda}h\cos\theta\right)}F^2(\theta) \tag{9}$$

For an EBG resonator antenna radiating broadside, the maximum power is in the direction of $\theta = 0$, and we find the equation regarding h determining the resonance,

$$\varphi - \pi - \frac{4\pi}{\lambda}h = -2N\pi \Longrightarrow h = \left(\frac{\varphi}{2\pi} - \frac{1}{2}\right)\frac{\lambda}{2} + N\frac{\lambda}{2}, \quad N = 0,\, 1,\, 2,\, \ldots \tag{10}$$

and the boresight gain relative to the feeding antenna

$$G = \frac{S}{F^2(\theta)} = \frac{1+\rho}{1-\rho} \tag{11}$$

As N increases, the antenna operating at higher modes, and consequently the sidelobes become higher. If the reflection phase of the PRS $\varphi = \pi$ and the antenna operates at the first resonant frequency, the distance h should be half a wavelength. Rearranging Equation (10) shows that for maximum gain within a certain frequency range the reflection phase of the PRS must satisfy the following relationship:

$$\varphi = \frac{4\pi h}{c}f - (2N-1)\,\pi, \quad N = 0,\, 1,\, 2,\, \ldots \tag{12}$$

It indicates that a PRS with a positive reflection phase gradient could yield a wideband EBG resonator antenna. The gain maximum will be determined by the magnitude of the reflection coefficient, ideally which should be constant according to Equation (11).

3. PRS WITH POSITIVE PHASE GRADIENT

According to the ray theory analysis in the previous section, an EBG structure with a linearly increasing phase response versus frequency is needed to yield a wideband EBG resonator antenna. Unfortunately, conventional EBG structures composed of 1-D dielectric slabs [16], 2-D printed FSSs [17] or 3-D woodpile structures [18], normally are with negative reflection phase slopes; thus, distinct schemes must be found for the construction of EBG structures to satisfy the phase relationship of Equation (12). One approach to realize this kind of EBG structure with 2-D printed FSSs has been reported, and the structures have been successfully applied to design wideband EBG resonator antennas [12–14]. In this section, we propose a method to realize this kind of EBG structure with 1-D dielectric slabs. The method will be described in detail by virtue of a transmission line model, and an EBG structure constructed with this approach will later be applied to the design of a wideband EBG resonator antenna.

The topology of the proposed EBG structure is illustrated in Fig. 2. It consists of two dielectric slabs spaced by a quarter wavelength

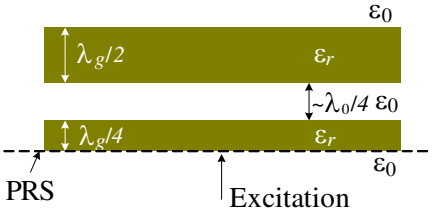

Figure 2. EBG structure.

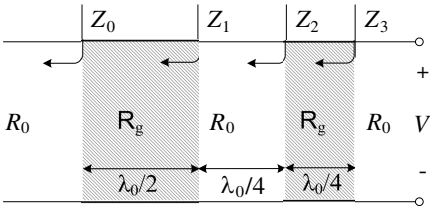

Figure 3. Transmission line model.

thick air-gap. The slabs are of the same dielectric constant and with thicknesses of half a guided wavelength and a quarter guided wavelength at center frequency f_c, respectively. Because the upper slab is twice as thick as the lower one, both slabs can be made of a single kind of dielectric substrate (stack two pieces together to form the upper one). This well facilitates the collection of fabrication materials. The lower surface of the EBG structure is used as the PRS and illuminated by a feeding antenna below. Assuming the structure is excited by plane waves, it can be equivalent to cascaded transmission lines, as shown in Fig. 3. Let the wave impedance of the air be R_0; thus the wave impedance in dielectric slabs is $R_g = R_0/\sqrt{\varepsilon}_r$. The open space above is modeled as a semi-infinite transmission line with characteristic impedance of R_0, which can also be treated as a broadband load R_0; the two slabs are modeled as transmission lines with characteristic impedance of R_g and lengths of half a wavelength and a quarter wavelength, respectively; similarly, the air-gap between the slabs is seen as a quarter wavelength transmission line with characteristic impedance of R_0. All the transmission lines are connected in series and the input impedance at each observation point, namely Z_0, Z_1, Z_2, and Z_3, can be calculated according to the transmission line theory. Thus we could obtain the reflection coefficient of the PRS, including the magnitude and phase response.

To better understand how the EBG structure produces a positive reflection phase slope, the Smith Chart is applied to visually exhibit the analysis procedure (from left to right) in terms of impedance transformation within a frequency range from $(f_c - \delta f)$ to $(f_c + \delta f)$. Firstly, as shown in Fig. 4(a), the position of $Z_0 = R_0$ on the Smith Chart normalized to R_g is a point on the right real axis because R_0 is frequency-independent, purely real, and larger than R_g; then Z_0 is clockwise rotated around the matching point by half a wavelength at f_c, producing curve Z_1. Secondly, normalize Z_1 to R_0; then curve Z_2 is obtained by rotating curve Z_1 clockwise around the matching point

by a quarter wavelength at f_c, as shown in Fig. 4(b). And similarly, Z_3 can be obtained by normalizing Z_2 to R_g, as shown in Fig. 4(c), and then rotating the curve clockwise by a quarter wavelength. Finally, the impedance curve Z_3 is renormalized to R_0 to calculate the reflection coefficient of the PRS and is shown in Fig. 4(d). It is worth noting that Z_1, Z_2 and Z_3. are frequency-dependent because the electrical lengths of transmission lines are proportional to frequency. In each step of the transformations, impedance points at higher frequencies travel further than those at lower frequencies, making curve Z_3 swirl near frequency f_c, resulting in a positive reflection phase slope within a small frequency range.

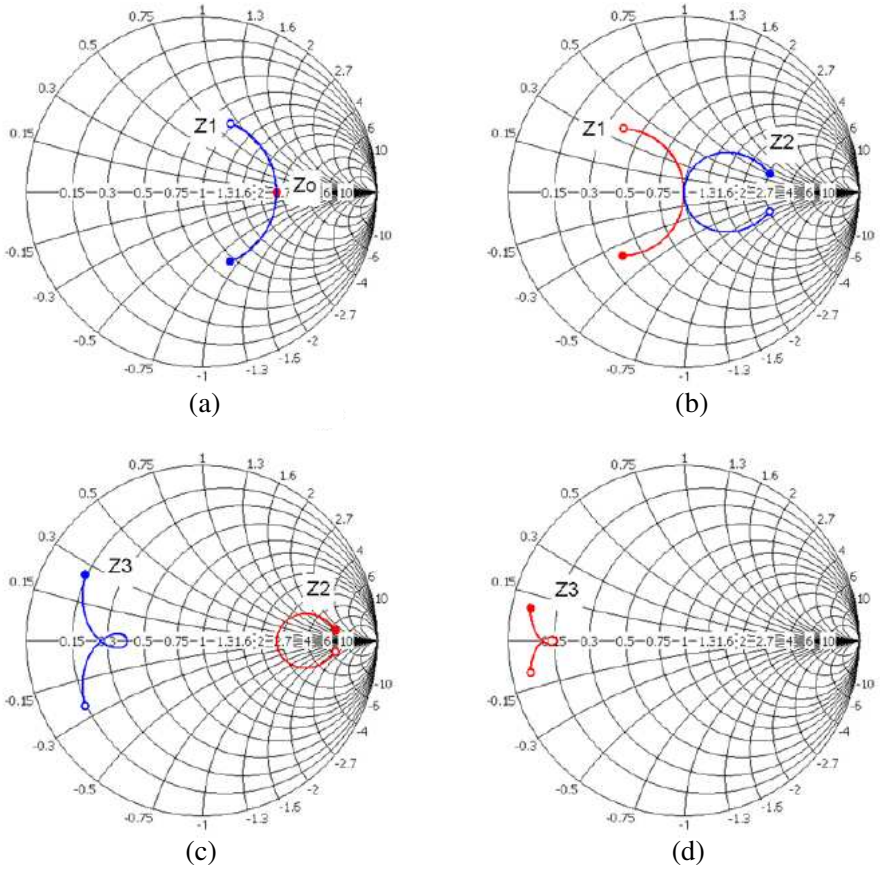

Figure 4. Impedance transformation ($\circ$: $f_c - \delta f, \bullet$: $f_c + \delta f$). (a) z_0 and z_1 normalized to R_g. (b) z_1 and z_2 normalized to R_0. (c) z_2 and z_3 normalized to R_g. (d) z_3 normalized to R_0.

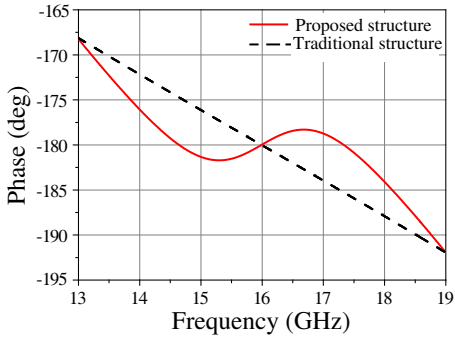

Figure 5. Reflection phase.

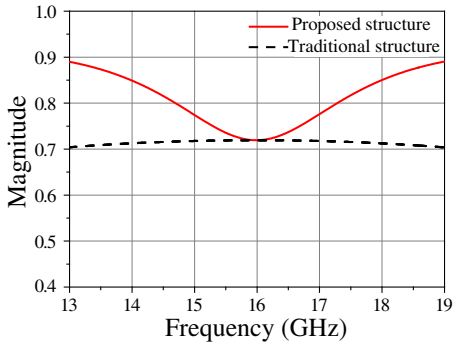

Figure 6. Reflection magnitude.

A practical design of this kind of EBG structure operating at Ku band is carried out based on the analysis. The Rogers RT/duroid 6006 substrate ($\varepsilon_r = 6.15$, $\tan\delta = 0.0027$) with thickness of 1.9 mm, which is a quarter guided wavelength thick at 16 GHz, is selected to construct the structure. Two pieces of the substrate are stacked up to form the upper layer, which is 3.8 mm thick. The air-gap between the two slabs is 4.7 mm. Fig. 5 and Fig. 6 show the phase and magnitude of the reflection coefficient calculated by the transmission line theory. For comparison purpose, the reflection phase and magnitude of a traditional EBG structure (made of a single layer of the same substrate) are also plotted. A positive phase gradient between 15.2 GHz and 16.8 GHz is observed for the proposed structure, while the traditional one is with a linearly decreasing phase response. The reflection magnitude of the proposed structure varies along the frequency, reaching the minimum value 0.72 at 16 GHz. In the following section, this EBG structure will be used for the realization of a wideband EBG resonator antenna.

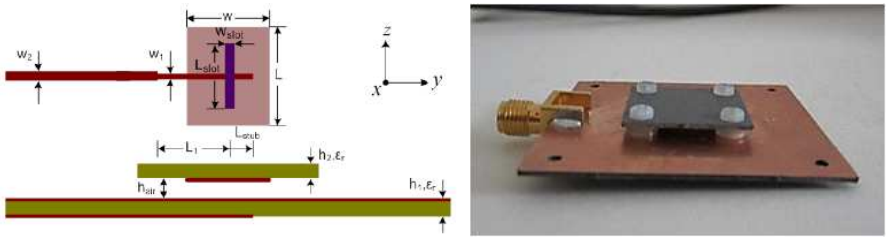

(a) (b)

Figure 7. Feeding antenna. (a) Structure and dimension. (b) Fabrication.

4. ANTENNA DESIGN

4.1. Feeding Antenna Design

Besides the EBG structure, the feeding antenna also plays an important role as the excitation of the EBG resonator antenna. In [11, 12, 14], a waveguide aperture in the ground plane, a probe-fed patch antenna, and a monopole suspended parallel to the ground plane by a distance, are chosen as feeding antennas, respectively. In our design, we choose the slot-coupled patch antenna as the candidate due to its low profile, ease of feeding and potential to have a wide bandwidth. The structure of the patch antenna is shown in Fig. 7(a). It is designed on the Rogers RT/duroid 5880 substrate ($\varepsilon_r = 2.2$, $\tan\delta = 0.0009$) with the thickness of 0.787 mm. The parasitic patch is coupled with the feed line through a slot in the ground plane, and it is spaced from the ground plane by an air-gap to suppress the excitation of surface waves which can be introduced to the cavity and degrade the performance of the EBG resonator antenna. A brief matching network is etched beneath the bottom layer to make the antenna provide a wide impedance bandwidth covering the operating band of the wideband EBG resonator antenna to be designed. The dimensions of the antenna are as follows: $W = 5.2\,\text{mm}$, $L = 5.2\,\text{mm}$, $W_1 = 1.2\,\text{mm}$, $W_2 = 2.3\,\text{mm}$, $L_1 = 5.5\,\text{mm}$, $W_{\text{slot}} = 1\,\text{mm}$, $L_{\text{slot}} = 5.6\,\text{mm}$, $L_{\text{stub}} = 2\,\text{mm}$, $h_{\text{air}} = 1.8\,\text{mm}$, $h_1 = h_2 = 0.787\,\text{mm}$.

This feeding antenna is firstly designed with the CST Microwave Studio 2011 and then fabricated and measured. An SMA (Sub-Miniature version A) connector is soldered to the feed line, as shown in Fig. 7(b). The simulated and measured reflection coefficients (S_{11}) are plotted in Fig. 8. Discrepancies exist between the two results. That is probably attributed to fabrication tolerance and poor performance of the SMA connector at Ku band. The measured result shows that

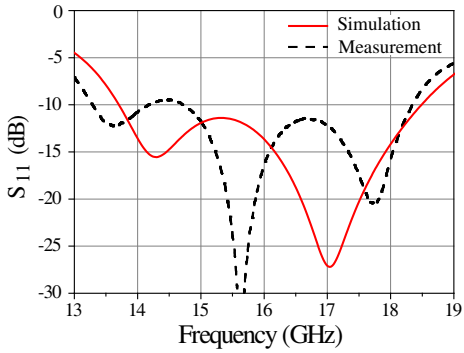

Figure 8. Reflection coefficient.

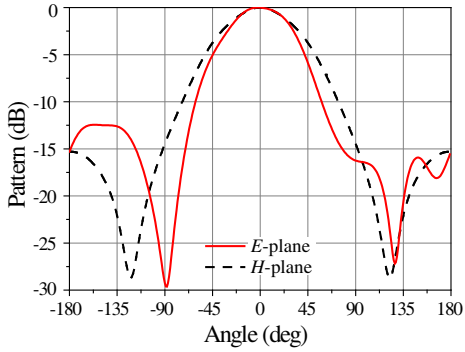

Figure 9. Simulated patterns at 16 GHz.

the antenna almost keeps $S_{11} < -10$ dB within the frequency range from 13.3 GHz to 18.3 GHz. Normalized radiation patterns of co-polarization in E-plane (yoz) and H-plane (xoz) at 16 GHz are plotted in Fig. 9. The antenna radiates broadside and has low back lobes less than -12 dB. Due to the satisfactory performances, this antenna will be used as the feeding antenna for the wideband EBG resonator antenna to be designed in the next section.

4.2. EBG Resonator Antenna Design

To form a wideband EBG resonator antenna, the EBG structure and the wideband feed antenna designed previously have to be combined together. Fig. 10(a) shows the structure of the EBG resonator antenna. The EBG structure is suspended above the feeding antenna and they share the same ground plane. All air-gaps are created by placing hex

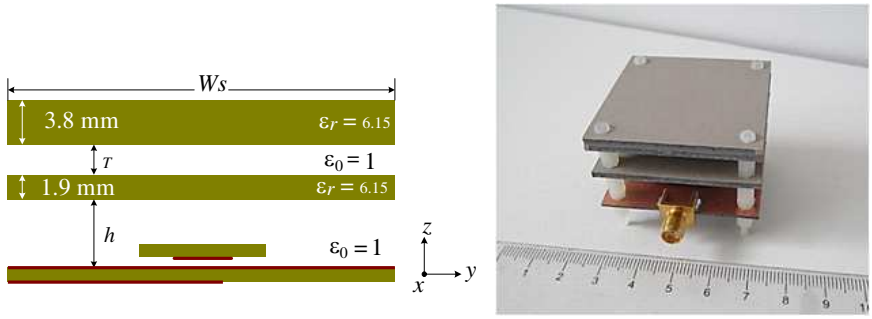

Figure 10. EBG resonator antenna. (a) Structure and dimension. (b) Fabrication.

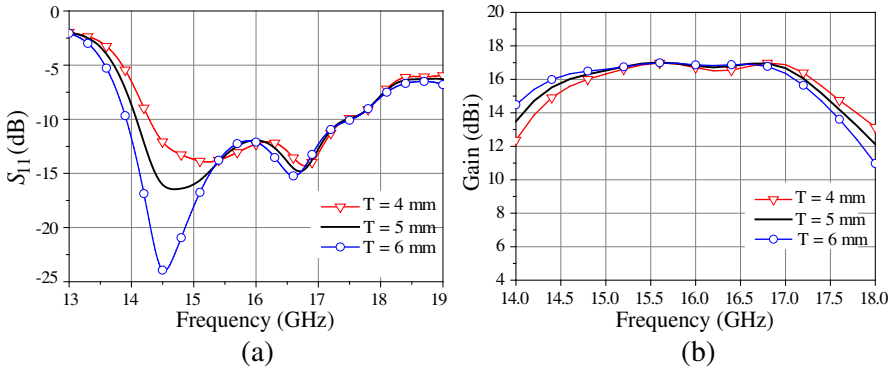

Figure 11. Parameter study of h, when $h = 10\,\text{mm}$. (a) Reflection coefficient. (b) Gain.

nylon spacers with the diameter of 2.3 mm and dielectric constant of 3 at four corners. The nylon spacers are also modeled and taken into account during the design process with CST Microwave Studio 2011. The lateral dimension of the antenna is 45 mm × 45 mm ($Ws \times Ws$), which is $2.4\lambda \times 2.4\lambda$ at 16 GHz.

Since the design of the EBG structure in Section 3 is based on the analysis of plane wave excitation, all thicknesses were exactly set to theoretical values at 16 GHz. However, the practical case is that waves from the feeding antenna are not plane ones; besides, the height of the feeding antenna may also impact the resonant frequency of the antenna. To reveal these impacts, parameter studies regarding the distance T between the two slabs and the resonance distance h, have been carried out. Fig. 11 shows the results of the parameter study of T

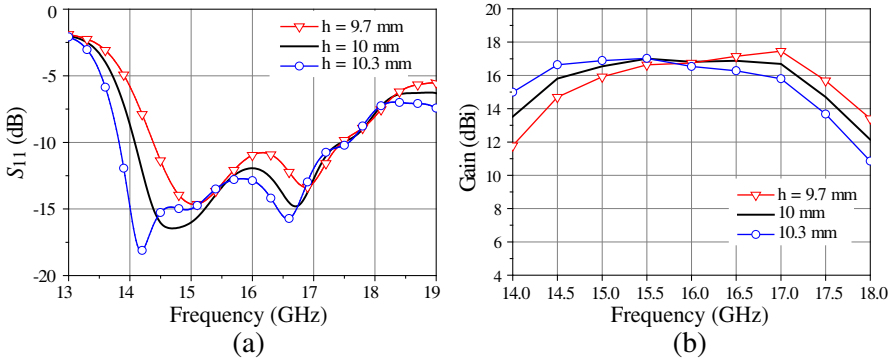

Figure 12. Parameter study of h, when $T = 5\,\text{mm}$. (a) Reflection coefficient. (b) Gain.

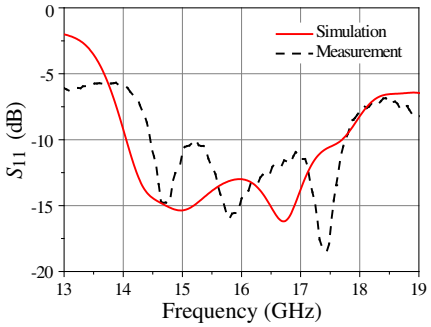

Figure 13. Reflection coefficient.

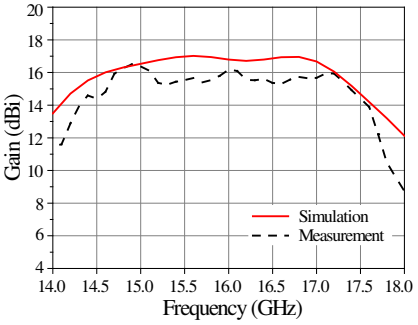

Figure 14. Antenna gain.

with $h = 10\,\text{mm}$. Within the frequency band from 14 GHz to 18 GHz, along with T increases from 4 mm to 6 mm, the impedance matching of the antenna at lower band becomes better and the directivity at lower band rises obviously, while those at higher band nearly remain unchanged, not as sensitive as those at lower band. The results of the parameter study of h with $T = 5\,\text{mm}$ are plotted in Fig. 12. It can be observed that, when h is increased, the impedance matching gets even better, and the gain bandwidth shifts downward. With $h = 10\,\text{mm}$ and $T = 5\,\text{mm}$, the gain curve is flat and the reflection coefficient (S_{11}) is satisfactory; the antenna has a 3 dB gain bandwidth of 22% (from 14.1 GHz to 17.6 GHz) with a maximum gain of 17 dBi, and an impedance bandwidth of 23% (from 14 GHz to 17.7 GHz) for $S_{11} < -10\,\text{dB}$, which can well cover the 3 dB gain bandwidth. Further, with these dimensions, a prototype is fabricated and assembled, as

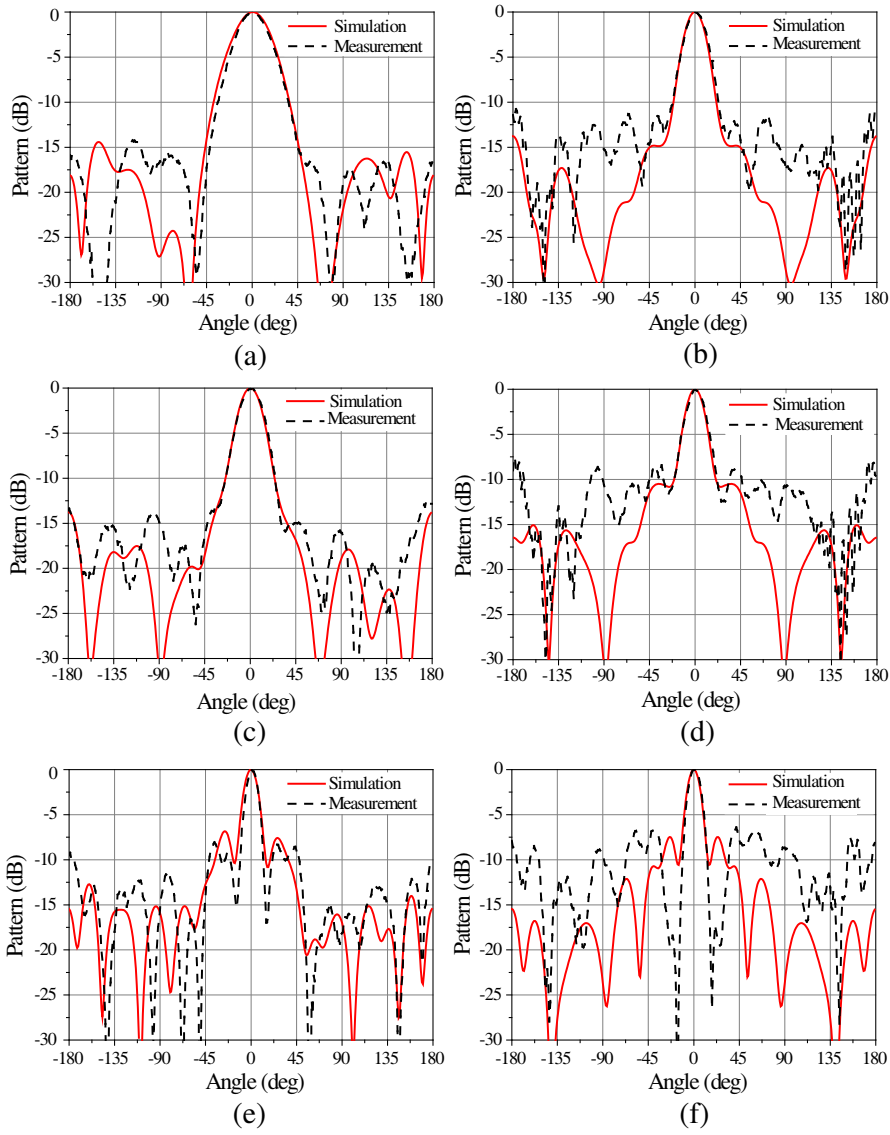

Figure 15. Radiation pattern. (a) E-plane at 15 GHz. (b) H-plane at 15 GHz. (c) E-plane at 16 GHz. (d) H-plane at 16 GHz. (e) E-plane at 17 GHz. (f) H-plane at 17 GHz.

shown in Fig. 10(b).

The reflection coefficient (S_{11}) of the antenna is measured with an Agilent Vector Network Analyzer (VNA) E8363B and plotted in Fig. 13. Discrepancies exist between the experimental and simulated results. The simulated impedance bandwidth for $S_{11} < -10\,\text{dB}$ covers the band from 14 GHz to 17.7 GHz (relatively 23%), while the measurement shows a impedance bandwidth from 14.5 GHz to 17.7 GHz (relatively 20%). This difference may be caused by the fabrication and assembly tolerances, and the bad performance of the SMA connector in Ku band.

The measurements of the antenna gain and radiation patterns are carried out in an anechoic chamber with a system based on an Agilent VNA E8363B. The measured gain is obtained by comparing measured power levels of the antenna with those of a reference horn antenna whose power levels and antenna gain are known in advance. Fig. 14 plots the simulated and measured antenna gain. The simulation shows that the 3 dB gain bandwidth is 22%, from 14.1 GHz to 17.6 GHz, and the peak gain is 17 dBi. Because of the metal loss and measurement error, the measured gain is slightly lower this calculated value, with a peak gain of 16.5 dBi. The measured gain bandwidth is from 14.3 GHz to 17.6 GHz (relatively 20.7%), narrower than the calculated value because the feed efficiency between 14 GHz and 14.5 GHz is worse than the simulation (see Fig. 13). It can be seen that the impedance band well covers the 3 dB gain band. Fig. 15 shows the E-plane (yoz) and H-plane (xoz) radiation patterns of the co-polarization at 15 GHz, 16 GHz and 17 GHz. Good agreements between the simulated and measured results are obtained except that sidelobes of the measured patterns are higher than those of the simulated ones. That is acceptable because at Ku band it is not easy to control the radiation of the cable and the SMA connector.

5. CONCLUSION

This paper firstly proposed an approach to use 1-D dielectric slabs, instead of metallic FSSs, to produce PRSs with positive reflection phase gradients. The structure is realized by a single kind of dielectric substrate, modeled as cascaded transmission lines, and analyzed by virtue of the Smith Chart from the perspective of impedance transformation. Then, a PRS designed by this approach is applied to the realization of a wideband EBG resonator antenna operating at Ku band which is fed by a wideband slot-coupled air-loaded patch antenna. The calculated results indicate that the antenna possesses a relative 3 dB gain bandwidth of 22%, from 14.1 GHz to 17.6 GHz,

with a peak gain of 17 dBi, while the measured gain bandwidth is from 14.3 GHz to 17.6 GHz (relatively 20.7%) with a maximum value of 16.5 dBi. Through the comparison between all the simulated and experimental results, the proposed method and the simulation have been well confirmed.

REFERENCES

1. Moustafa, L. and B. Jecko, "EBG structure with wide defect band for broadband cavity antenna applications," *IEEE Antennas and Wireless Propagation Letters*, Vol. 7, 693–696, 2008.
2. Leger, L., C. Serier, R. Chantalat, M. Thevenot, T. Monediere, and B. Jecko, "1D dielectric electromagnetic band gap (EBG) resonator antenna design," *Annales des Télécommunications*, Vol. 59, No. 34, 242–260, Mar.–Apr. 2004.
3. Costa, F. and A. Monorchio, "Design of subwavelength tunable and steerable Fabry-Perot/leaky wave antennas," *Progress In Electromagnetics Research*, Vol. 111, 467–481, 2011.
4. Pirhadi, A., F. Keshmiri, M. Hakkak, and M. Tayarani, "Analysis and design of dual band high directive EBG resonator antenna using square loop FSS as superstrate layer," *Progress In Electromagnetics Research*, Vol. 70, 1–20, 2007.
5. Feresidis, A. P., G. Goussetis, S. Wang, and J. C. Vardaxoglou, "Artificial magnetic conductor surfaces and their application to low-profile high-gain planar antennas," *IEEE Transactions on Antennas and Propagation*, Vol. 53, No. 1, 209–215, Jan. 2005.
6. Vettikalladi, H., O. Lafond, and M. Himdi, "High-efficient and high-gain superstrate antenna for 60-GHz indoor communication," *IEEE Antennas and Wireless Propagation Letters*, Vol. 8, 1422–1425, 2009.
7. Rodes, E., M. Diblanc, E. Arnaud, T. Monediere, and B. Jecko, "Dual-band EBG resonator antenna using a single-layer FSS," *IEEE Antennas and Wireless Propagation Letters*, Vol. 6, 368–371, 2007.
8. Leger, L., T. Monediere, and B. Jecko, "Enhancement of gain and radiation bandwidth for a planar 1-D EBG antenna," *IEEE Microwave and Wireless Components Letters*, Vol. 15, No. 9, 573–575, Sep. 2005.
9. Moustafa, L. and B. Jecko, "Design of a wideband highly directive EBG antenna using double-layer frequency selective surfaces and multifeed technique for application in the Ku-band," *IEEE Antennas and Wireless Propagation Letters*, Vol. 9, 342–346, 2010.

10. Weily, A., K. P. Esselle, T. S. Bird, and B. C. Sanders, "Dual resonator 1-D EBG antenna with slot array feed for improved radiation bandwidth," *IET Microwaves, Antennas & Propagation*, Vol. 1, No. 1, 198–203, Feb. 2007.
11. Feresidis, A. P. and J. C. Vardaxoglou, "High gain planar antenna using optimized partially reflective surfaces," *IEE Proceedings on Microwaves, Antennas and Propagation*, Vol. 148, No. 6, 345–350, Dec. 2001.
12. Moustafa, L. and B. Jecko, "Design and realization of a wide-band EBG antenna based on FSS and operating in the Ku-band," *International Journal of Antennas and Propagation*, Vol. 2010, 8 pages, Article ID 139069, 2010.
13. Feresidis, A. P. and J. C. Vardaxoglou, "A broadband high-gain resonant cavity antenna with single feed," *First European Conference on Antennas and Propagation, EuCAP 2006*, 1–5, Nov. 2006.
14. Ge, Y., K. P. Esselle, and T. S. Bird, "The use of simple thin partially reflective surfaces with positive reflection phase gradients to design wideband, low-profile EBG resonator antennas," *IEEE Transactions on Antennas and Propagation*, Vol. 60, No. 2, 743–750, Feb. 2012.
15. Trentini, G. V., "Partially reflecting sheet arrays," *IEEE Transactions on Antennas and Propagation*, Vol. 4, No. 4, 666–671, Oct. 1956.
16. Zeb, B. A., Y. Ge, K. P. Esselle, Z. Sun, and M. E. Tobar, "A simple dual-band electromagnetic band gap resonator antenna based on inverted reflection phase gradient," *IEEE Transactions on Antennas and Propagation*, Vol. 60, No. 10, 4522–4529, Oct. 2012.
17. Vaidya, A. R., R. K. Gupta, S. K. Mishra, and J. Mukherjee, "High-gain low side lobe level fabry perot cavity antenna with feed patch array," *Progress In Electromagnetics Research C*, Vol. 28, 223–238, 2012.
18. Lee, Y., X. Lu, Y. Hao, S. Yang, J. Evans, and C. G. Parini, "Low-profile directive millimeter-wave antennas using free-formed three-dimensional (3-D) electromagnetic bandgap structures," *IEEE Transactions on Antennas and Propagation*, Vol. 57, No. 10, 2893–2903, Oct. 2009.